Chemical Science

ROYAL SOCIETY OF CHEMISTRY

EDGE ARTICLE

View Article Online
View Journal | View Issue

Cite this: *Chem. Sci.*, 2026, **17**, 1051

All publication charges for this article have been paid for by the Royal Society of Chemistry

Received 28th February 2025
Accepted 3rd November 2025

DOI: 10.1039/d5sc01631b

rsc.li/chemical-science

Generation of reactive oxygen species in water droplets levitated in air

Yu Xia, [ac] Xiaoxu Li,[b] Fengjie Chen,[a] Jinheng Xu, [c] Xufeng Gao,[b] Bolei Chen, *[ad] Xinxing Zhang *[b] and Richard N. Zare *[c]

Water droplets exceeding 100 μm in diameter are commonly found in natural aerosols, where the surfaces of these droplets often acquire charges owing to contact and friction with the surrounding air and particulates, influencing various atmospheric processes. This study reports the generation of reactive oxygen species (ROS) in millimeter-sized droplets levitated in air. The friction between the droplets and air results in positive charge accumulation on the droplet surface, which leads to ROS production from the water while smaller, negatively charged droplets escape from the surface. The concentration of ROS increases with droplet suspension time. Under electrostatic fields, such as those present in cumulonimbus clouds, corona discharge occurs on the droplet surface, further enhancing ROS formation. These findings offer a new mechanistic explanation for the presence of ROS in raindrops, arising from chemical processes at the charged air–water interface of atmospheric droplets.

Introduction

Water droplets, commonly present in clouds, mist, and aerosols, play a pivotal role in atmospheric processes and air quality control.[1–7] These droplets typically range in size from a few micrometers to several millimeters in diameter.[8] Recent research has highlighted unique chemical phenomena at the gas–liquid interface of microdroplets, generally defined as those with diameters below ~60 μm, including markedly accelerated reaction rates and a broad spectrum of redox processes. In contrast, larger droplets (hundreds of micrometers to millimeters) display distinct physicochemical characteristics, such as complex internal circulation and highly dynamic interfacial behavior, which remain comparatively less explored. By adopting this established size threshold, we seek to clearly delineate the well-studied domain of microdroplets from the millimeter-sized droplets that constitute the focus of the present study.[9–12]

The chemical behavior of millimeter-sized droplets, which exhibit significant internal flows and positive charging, remains poorly understood.[13,14] Unlike microdroplets, which maintain relatively uniform internal flow caused by surface tension, millimeter-sized droplets exhibit more complex internal dynamics, which results in a highly dynamic gas–liquid interface.[15] This internal flow leads to continuous friction between the droplet and the surrounding air, causing the droplet to acquire a positive charge, a phenomenon consistent with contact electrification principles.[16,17]

Despite these advancements, the impact of contact electrification on the interfacial chemical processes in millimeter-sized droplets has yet to be extensively investigated. In this study, we explore the gas–liquid interfacial chemistry of aqueous millimeter droplets levitated in air, focusing on how the evolution of surface charge influences these processes.

Previous studies have shown that electrons in water molecules can escape from the droplet surface during interactions with surrounding materials, including the gas phase.[16] Our earlier work demonstrated that electron transfer from water to solid surfaces, coupled with the formation of interfacial electric fields induced by water–solid contact electrification, can drive redox reactions at the interface.[17–19] Based on these findings, we hypothesize that the contact electrification of aqueous droplets with air could similarly influence interfacial chemical processes. Understanding the physicochemical processes governing electron loss from the hydrogen-bonded network in millimeter droplets is therefore crucial for advancing our knowledge of water droplet chemistry.

It is important to note that reaction acceleration is not universal across all droplet systems, with some studies reporting minimal effects even in smaller droplets.[20] Therefore, the phenomena observed in millimeter-sized droplets may arise

[a]*Hubei Key Laboratory of Environmental and Health Effects of Persistent Toxic Substances, School of Environment and Health, Jianghan University, Wuhan, 430056, China*

[b]*College of Chemistry, State Key Laboratory of Advanced Chemical Power Sources, Tianjin Key Laboratory of Biosensing and Molecular Recognition, Frontiers Science Centre for New Organic Matter, Nankai University, Tianjin, 300071, China. E-mail: zhangxx@nankai.edu.cn*

[c]*Department of Chemistry, Stanford University, Stanford, CA 94305, USA. E-mail: zare@stanford.edu*

[d]*State Key Laboratory of Environmental Chemistry and Toxicology, Research Center for Eco-environmental Sciences, Chinese Academy of Sciences, Beijing, 100085, China. E-mail: blchen@rcees.ac.cn*

from distinct mechanisms, such as their extended lifetimes and the dynamic charge separation described herein, rather than from factors dominant at smaller scales (*e.g.*, extreme curvature).[21]

Results and discussion

To model an aqueous millimeter droplet dynamically levitated in air, we used an acoustic levitator comprising an ultrasonic transmitter and a reflector, which was inspired by previous work.[10,22] The acoustic field generated by these arrays successfully levitated a millimeter-sized droplet with a diameter of 1.5 mm (Fig. 1A), using an ultrasonic frequency of 38.5 kHz. The entire experimental setup was enclosed in a sealed plastic chamber to minimize large-scale convective air currents that could displace the droplet. However, the localized air motion generated by the acoustic field was maintained, ensuring a stable yet dynamic gas–liquid interface essential for droplet levitation and interfacial interactions. The acoustic pressure field between the transmitter arrays was simulated using the COMSOL Multiphysics software, with a typical wave node highlighted by the black circle in Fig. 1B. When the droplet was positioned at one of these nodes, the upward force exerted by the acoustic field counterbalanced the droplet's gravitational force (Fig. S1), enabling it to remain levitated.

A water-soluble probe (10-acetyl-3,7-dihydroxyphenoxazine) was used to detect the generation of reactive oxygen species (ROS) in the droplet levitated in air. As shown in Fig. 1C, a strong orange fluorescence emission was observed from the floating droplet containing the probe under 530 nm laser excitation. This observation suggests that the spontaneous generation of ROS occurs not only in sprayed microdroplets (diameter < 60 μm), as extensively studied before,[9,23] but also in floating millimeter droplets. The generation of ROS in the droplets was further confirmed by using potassium titanium oxalate (PTO; $K_2TiO(C_2O_4)_2 \cdot H_2O$) according to a previously reported method,[9,19] as shown in Fig. 1D and S2. ROS with an oxidation capacity comparable to that of hydrogen peroxide at a concentration of 16 μM were detected in the droplet. As shown in Fig. S3, the generation of hydroxyl radicals was confirmed by the mass spectrum of the levitated droplets.

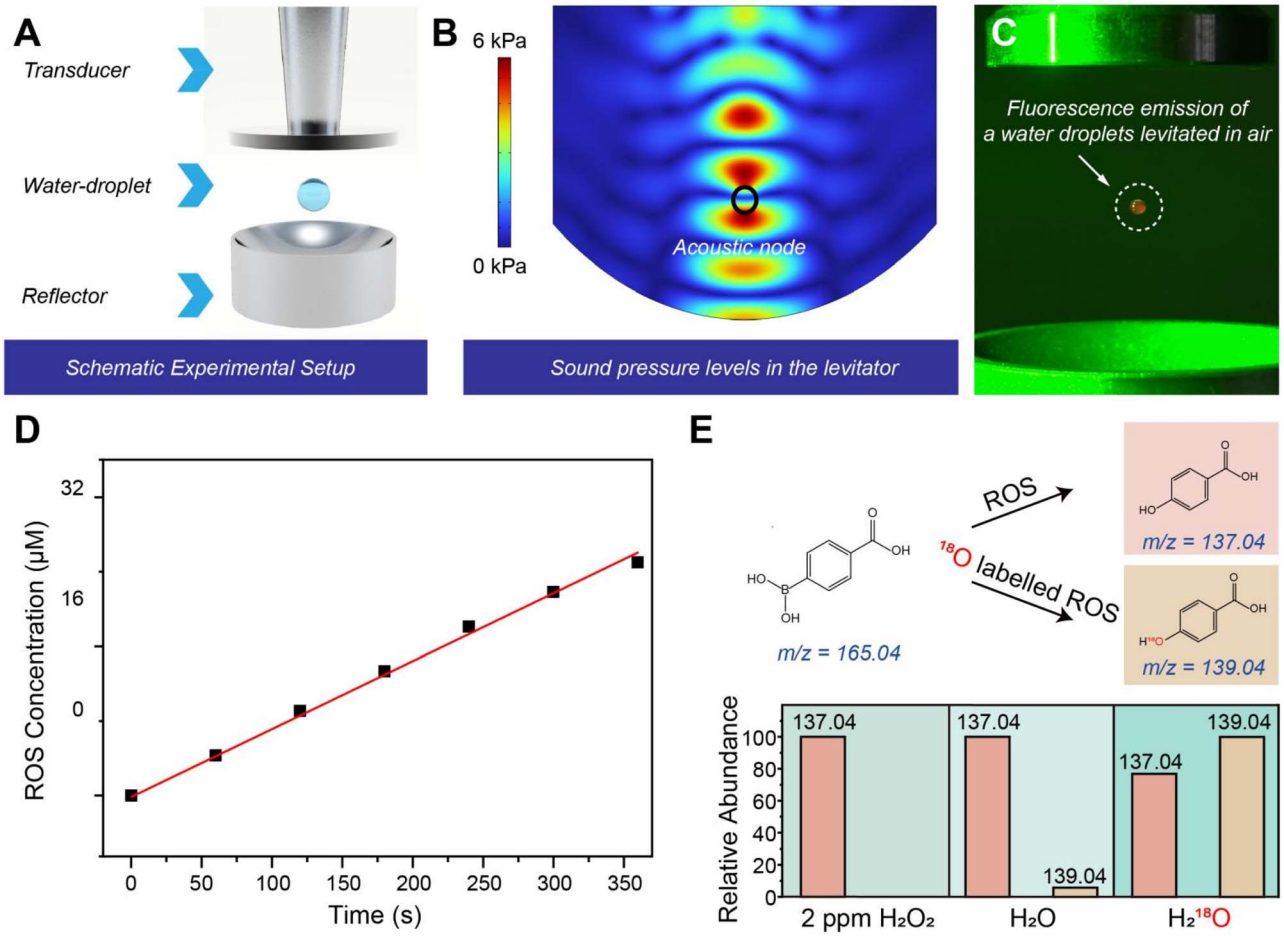

Fig. 1 (A) Schematic experimental setup of the acoustic levitator. (B) Sound pressure level in the levitator. (C) Digital image of fluorescence emission of the droplet. (D) A typical relationship between ROS concentration a suspension time. (E) Mass spectrum analysis of 4-hydroxybenzoic acid in the H_2O_2, levitated H_2O and $H_2{}^{18}O$ droplets. Data points represent the mean ± standard deviation from three independent replicate measurements ($n = 3$). The PTO assay was confirmed to be linear under the experimental conditions used.

To identify the origin of ROS in the droplet, we examined water droplets containing heavy oxygen ($H_2{}^{18}O$). Which were levitated in air for 10 minutes. The generated ROS in the droplet was reacted with 4-carbonxyphenylboronic acid (4-CPB) (Fig. S4). By comparing the mass spectra of 4-hydroxybenzoic acid productions from commercial H_2O_2, levitated H_2O and $H_2{}^{18}O$ droplets, the observed increase in the peak at 139.04 m/z indicates that the O atoms in ROS originate from $H_2{}^{18}O$ in the droplet, as shown in Fig. 1E. Additionally, the simultaneous generation of both ^{16}O-labeled (137.04 m/z) and ^{18}O-labeled (139.04 m/z) products with comparable signal intensities were observed in $H_2{}^{18}O$ droplets. This result can be attributed to the abundant lighter isotopic water molecules ($H_2{}^{16}O$) present on the surface of the heavy water, which could mitigate the expected isotopic effect of $H_2{}^{18}O$ on the redox reactions.[19]

To elucidate the relationship between the dynamic gas–liquid interface of millimeter droplets and ROS generation, we first simulated the internal flow within the droplets. As shown in Fig. S5, the interplay between the air flow induced by the acoustic pressure and the surface tension of the droplet created an internal vortex, resulting in continuous air–liquid friction. Millimeter-scale droplets (~2 mm in diameter) were levitated to investigate their interfacial dynamics and the resulting ROS generation. The dynamic behavior of the floating millimeter droplet was captured using a high-speed camera. Notably, we observed the motion of a microbubble within the droplet (Video S1), marked by the yellow dashed circle in Fig. 2A. The motion of this microbubble provides evidence of the internal vortices and air–water friction at the droplet's surface. Simultaneously, the fluorescence of the levitated droplet was captured using the high-speed camera. As shown in Fig. 2B, S6, and Video S2, the fluorescence intensity emitted by the droplet increased with prolonged suspension time. These droplets are substantially larger than typical microdroplets, and their internal circulation and interfacial dynamics therefore differ accordingly.

The detection of ROS using these probes is well-established, yet each method has specific characteristics that warrant consideration. 10-Acetyl-3,7-dihydroxyphenoxazine (Amplex Red) is highly specific for ROS,[24] while potassium titanium oxalate (PTO) provides a robust colorimetric assay for the same analyte.[25] 4-Carboxyphenylboronic acid (4-CPB) selectively reacts with hydroxyl radicals to form a phenolic product.[9] To ensure reliability, calibration curves were constructed for each assay to confirm a linear response within the measured concentration range. The convergent results obtained from these orthogonal methods significantly reduce the likelihood of false positives. Furthermore, control experiments with non-levitated samples and reagent blanks were consistently performed to account for any background signal or non-specific reactions.

Subsequently, we measured the real-time charge on the levitated droplet. A gold probe was inserted into the droplet, and the electrical signal from the probe was measured with an electrometer. As shown in Fig. S7, the millimeter droplet exhibited a net positive charge,[26] contrasting with a previous finding where sprayed microdroplets with diameters less than 60 μm were typically negatively charged. The charge accumulation rate of the levitated droplet is about 0.125 nC s^{-1}. Notably, we do not interpret that the increasing charge transfer curve without saturation indicates a continued accumulation of positive charge on the droplet surface. Instead, this result was caused by the transfer of droplet surface charge through the metal probe to the electrometer. Fig. 2C shows a linear relationship between the accumulated positive charge on the levitated droplet surface and the enhancement of fluorescence intensity, consistent with the hypothesis that charge transfer at the droplet–air interface promotes ROS generation, while the underlying mechanism awaits further investigation. To further investigate the surface charge transfer mechanism in the millimeter droplet, we quantified the charge transfer on the surface of the levitated droplet under controlled variations in temperature, humidity, and atmospheric composition. As shown in Fig. 2D, the amount of charge transfer on the droplet surface increases significantly as the temperature rises from 20 °C to 40 °C. This trend likely reflects several coupled factors: (1) elevated temperatures enhance charge exchange during air–water friction, (2) accelerated evaporation promotes the release of fine negatively charged droplets, and (3) reduced viscosity and surface tension at higher temperatures facilitate internal circulation and surface deformation, thereby increasing the effective interfacial area for charge exchange. Fig. 2E shows that the amount of charge transfer on the droplet surface decreases slightly with increasing humidity. This effect may be attributed to the higher water vapor content in the air, which increases its viscosity and hinders the release of fine droplets. Fig. 2F shows that the composition of the atmosphere surrounding the levitated droplet also affects the charge transfer on its surface. The amount of charge transfer in air is higher than that in methane and nitrogen, which can be attributed to the differing electron affinities of these gases, a finding that aligns with previous studies.[22] Additionally, we propose that the generation of ROS in the levitated millimeter droplet arises from the ultra-strong electric field established between the net positive charge on its surface and the negatively charged fine droplets released during evaporation. This hypothesis is primarily supported by the strong linear correlation observed between the accumulated positive charge and the increase in ROS production (Fig. 2C). It is important to qualify that the charge measurement, conducted *via* insertion of a gold probe, could theoretically be influenced by factors such as trace surface contaminants, although rigorous cleaning protocols were employed. However, the systematic dependence of the charge signal on environmental conditions (Fig. 2D–F), coupled with its direct correlation with an independent measure of ROS, strongly suggests that the measured trend robustly reflects a physical phenomenon intrinsic to the droplet–air interaction. Therefore, we conclude that the friction-induced charge separation and the associated interfacial electric field are the dominant drivers of ROS generation in this system.

It might be wondered whether acoustic cavitation or direct ultrasonic irradiation affect the results we report. To test this hypothesis, we added another set of ultrasonic generators to the original experimental setup, and its structure is shown in Fig. S8A. The ultrasonic generator parallel to the direction of

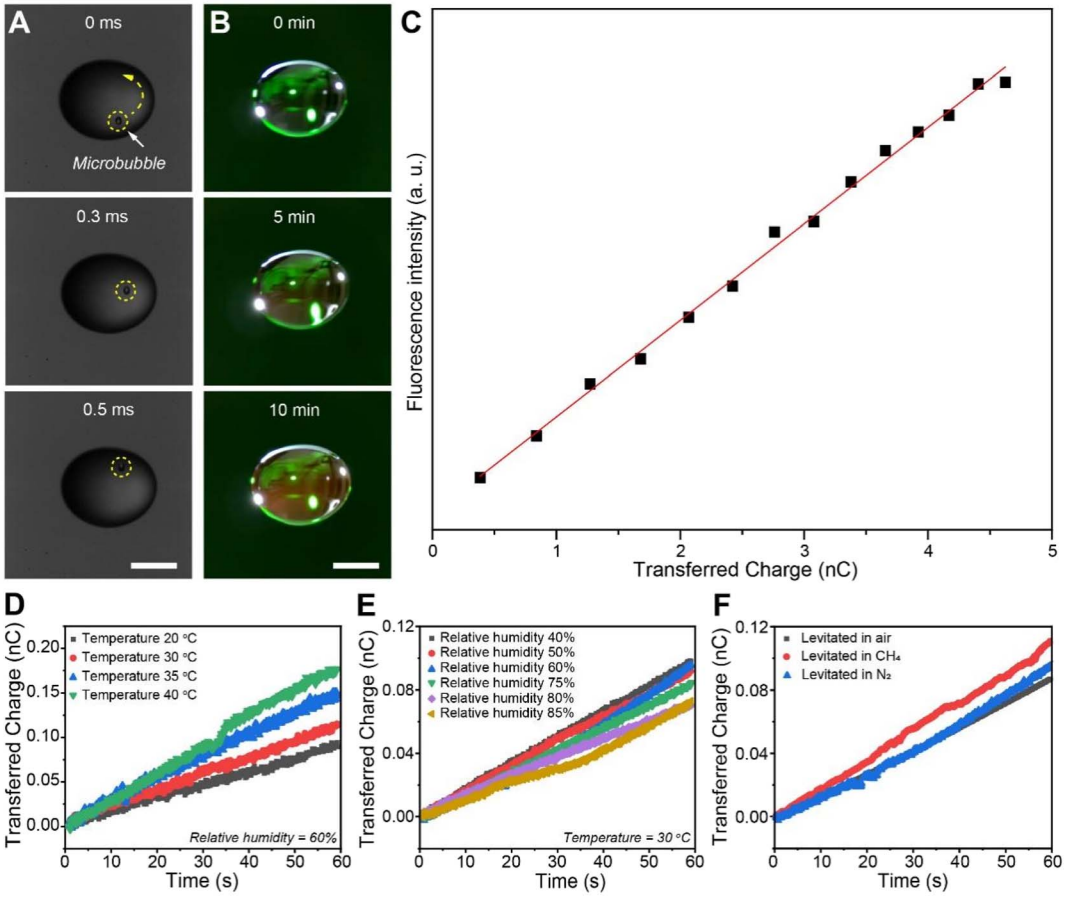

Fig. 2 (A) A microbubble rotating at high speed in the droplet. (B) Increase of fluorescence emission of the droplet depended on levitated time. (C) Lineal relationship between fluorescence intensity and transferred charge of the droplet. (D) Transferred charge increase at different environmental temperatures. (E) Transferred charge increase at different relative humidity. (F) Transferred charge increase in different atmosphere. The scale bars are 1 mm for both panel A and B.

gravity is used to counteract the effect of gravity and suspend the liquid droplets. Ultrasonic waves perpendicular to the direction of gravity exert another sound field force on the droplet. We compared fluorescence signals of ROS generated from droplets in two experimental setups and found that their ROS concentration was at the same level, as shown in Fig. S8B. This result indicates that the fluorescence signal of the droplet we observed mainly comes from the interaction between the droplet and the air.

In the atmosphere, millimeter-sized droplets are found most commonly in cumulonimbus and stratus clouds. There is no doubt that we need to consider the influence of electric fields in cumulonimbus clouds on the interfacial chemistry of charged droplets. Given that electric field intensities in cumulonimbus clouds range from a few kV m^{-1} to several hundred kV m^{-1}, we placed a levitated droplet in an electrostatic field (30 kV m^{-1}). As shown in Fig. 3A and B, we observed a typical corona discharge on the side of the droplet surface near the negative electrode after 70 ms of suspension. This discharge persisted for 8 ms. Following the discharge, the droplet recharged itself over 2 ms, after which a second corona discharge occurred. As shown in Fig. 3C and Video S3, this process repeated cyclically. Additionally, we observed a weaker corona discharge on the side of the droplet near the positive electrode (Fig. S9 and Video S3). This phenomenon can be attributed to the fact that the levitated millimeter droplet is positively charged, and the polarization electric field intensity, resulting from the accumulation of positive charge under the influence of an external electrostatic field, is significantly higher than that of the negative charge. Corona discharge from a charged sphere in an electrostatic field is intrinsically complex. Small deviations from perfect symmetry in droplet shape or surface condition can cause one side of the droplet to initiate discharge first. Once discharge begins, the resulting redistribution of the local electric field can reinforce this asymmetry, allowing the initially discharging site to remain dominant. For a charged sphere, discharge rarely occurs exclusively at a single location; more commonly, two discharge points are formed with unequal intensities. It is worth noting that previous studies have reported corona discharge phenomena on the surfaces of microdroplets.[21] While corona discharges can occur on both millimeter-sized droplets and microdroplets, we propose that they arise from different physical mechanisms. In millimeter-sized droplets, the discharge is primarily driven by the accumulation of positive

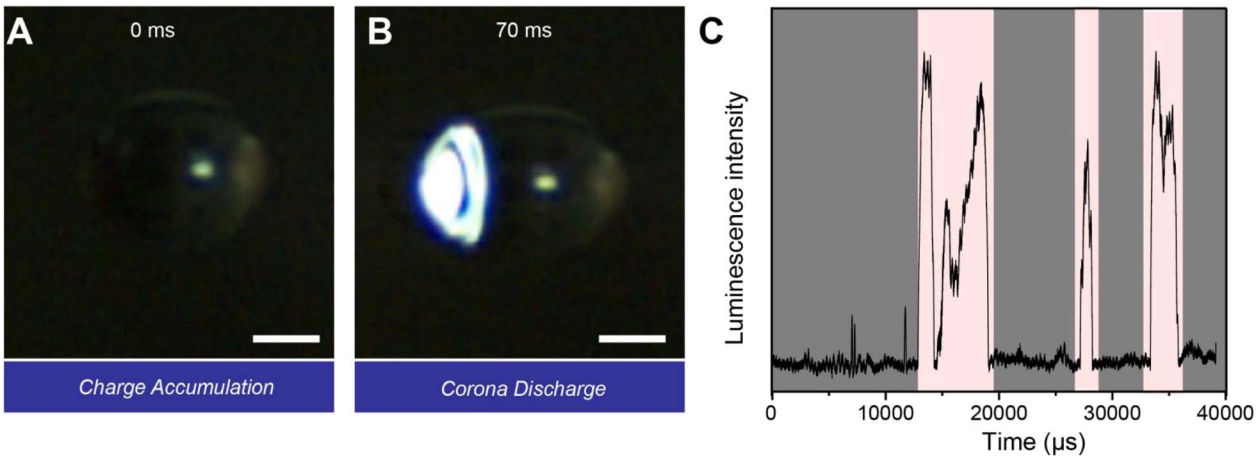

Fig. 3 (A) Digital image of the initial state of a levitated droplet in an electrostatic field. (B) Digital image of corona discharge on the surface of levitated droplet placed in an electrostatic field. (C) Charge and discharge on the surface of the levitated droplet repeated cyclically. The scale bars are 1 mm for both panel A and B.

charges generated through water–air contact electrification. In contrast, the discharge observed in microdroplets stems from the build-up of negative charges. These findings suggest that multiple physicochemical processes may coexist at the water droplet interface, collectively influencing its charging behavior and subsequent redox reactions.

We have also examined how the change in droplet size affects ROS generation. As shown in Fig. S10, we observed the reactions of ROS generation in droplets with diameters of 2000, 1500, 1000, and 500 μm respectively. The fluorescence intensity of its ROS-sensitive probe decreases as the droplet diameter decreases. However, it is difficult for us to simply attribute this phenomenon to the change in droplet size. This is because when the size of the droplet decreases, the gravitational force of the droplet reduces. To ensure its stable suspension, we must lower the power of the ultrasonic generator to balance the forces acting on the droplet. Although the previous experiments confirmed that the change of ultrasonic power has a limited influence on the ROS generation process, the reduction of ultrasonic power can also lead to a decrease in the air flow velocity around the droplets. In addition, as the droplet size decreases, the influence of its surface tension on the interfacial flow of the droplet increases, which also affects the interaction between the droplet and the air. Therefore, the change in droplet size leads to the variation of multiple dependent variables in the entire experimental system.

To evaluate the effect of droplet discharge on the generation of ROS, we examined the fluorescence intensity of droplets containing ROS fluorescent probes. As shown in the Fig. 4A, when a droplet was levitated in the electrostatic field for 10 min, its fluorescence intensity is significantly higher than that of a droplet levitated without the presence of the electrostatic field. Quantitative analysis of ROS based on their reaction with PTO shows that the concentration of ROS in the levitated droplet is comparable with the H_2O_2 solution with concentration of 18 μM in the absence of electrostatic field, while the concentration of ROS doubled in the droplet levitated in the electrostatic field (Fig. 4B). As shown in Fig. 4C, we measured the generation of hydroxyl radicals ($^{\bullet}OH$) and superoxide radical anions ($^{\bullet}O_2^-$) with and without an applied electrostatic field, respectively. Quantitative comparison is supported by the consistent experimental conditions and the clear relative intensity changes observed between samples.[27] Electron spin resonance spectra show that the signals of these two kinds of free radicals increase obviously in the presence of electrostatic field. In general, these results suggest that the radical generation observed in the levitated millimeter-sized droplet may be induced by the ultra-strong electric field at the water–air interface, which is in good agreement with our previous works.[20]

To further understand the potential correspondence between our model and natural phenomena, we used COMSOL software to simulate the air flow field around the levitated droplets. Our results indicate that the air flow rate surrounding the droplet is approximately 2–10 m s^{-1} (Fig. S11). Furthermore, if we assume that the microbubble in the droplet moves along the surface of the droplet sphere (shown in Fig. 2A and Video S1), the bubble in the droplet moves at a speed of 2 m s^{-1}. Therefore, our model aligns with the behavior of droplets in the atmosphere under strong breeze conditions.[22] Given that the bottom of a cumulonimbus cloud is typically negatively charged, we hypothesized that the ROS generation process caused by electric field at millimeter droplet surface, as observed in the laboratory, also occurs in raindrops within cumulonimbus clouds, particularly as they gravitationally approach the bottom of the clouds. Whereas stratospheric ozone (O_3) is thought to arise from the UV photodissociation of O_2, tropospheric ozone is usually attributed to chemical reactions between oxides of nitrogen (NO_x) and volatile organic compounds (VOC), which occur when pollutants chemically react in the presence of sunlight. The present study offers yet a different mechanism, namely, electrical discharge of the droplets, which can take place in the dark as well as in sunlight.[23]

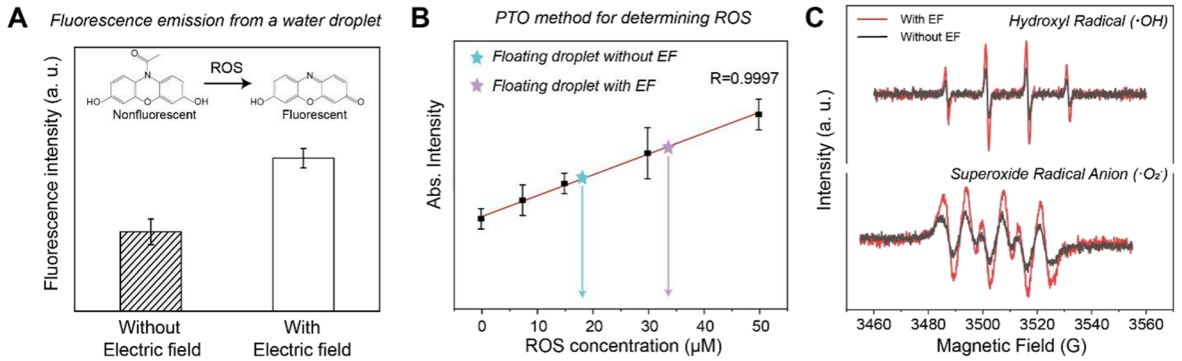

Fig. 4 (A) Fluorescence intensity profiles of ROS generation in droplet levitated with and without electric field. (B) Corresponding ROS concentration in droplet levitated with and without electric field. (C) Corresponding ESR spectra of radicals generated in droplet levitated with and without electric field. Data points represent the mean ± standard deviation from three independent replicate measurements ($n = 3$). The PTO assay was confirmed to be linear under the experimental conditions used.

Conclusions

In conclusion, our study provides strong evidence that reactive oxygen species (ROS) are generated in levitated millimeter droplets. These droplets acquire a net positive charge, and when placed in an electrostatic field, a corona discharge is observed at the droplet surface. This discharge process further enhances ROS generation. We propose that the generation of ROS is driven by the ultra-strong electric field at the dynamic liquid–gas interface of millimeter-sized droplets as they float in air. This discovery not only deepens our understanding of chemical reactions occurring at aqueous interfaces but also reveals previously unrecognized chemical processes that may take place in clouds and raindrops.

Author contributions

Y. X., B. C., X. Z. and R. N. Z. designed research; Y. X., X. L., F. C., J. X., and X. G. performed research. Y. X., B. C., X. Z. and R. N. Z. analysed data and wrote the paper.

Conflicts of interest

There are no conflicts to declare.

Data availability

The data supporting this article have been included as part of the SI. Supplementary information: including experimental details, Fig. S1 to S11 and Videos S1 to S3. See DOI: **https://doi.org/10.1039/d5sc01631b**.

Acknowledgements

X. Z. acknowledges the National Key R&D Program of China (2023YFE0124200), the National Natural Science Foundation of China (22325402 & 22174073), the NSF of Tianjin City (21JCJQJC00010), the NCC Fund (NCC2022PY05), the Haihe Laboratory of Sustainable Chemical Transformations, and the Frontiers Science Center for New Organic Matter at Nankai University (63181206). B. C. acknowledges the National Natural Science Foundation of China (22193051, 22193052, 22306073 and 22376080), and the Hubei Provincial Natural Science Foundation of China (2024AFA089). R. N. Z. acknowledges the US Air Force Office of Scientific Research through the Multi-disciplinary University Research Initiative (MURI) program (AFOSR FA9550-21-1-0170).

Notes and references

1 D. Rosenfeld, S. Sherwood, R. Wood and L. Donner, *Science*, 2014, **343**, 379–380.
2 S. Bony, B. Stevens, D. M. W. Frierson, C. Jakob, M. Kageyama, R. Pincus, T. G. Shepherd, S. C. Sherwood, A. P. Siebesma, A. H. Sobel, M. Watanabe and M. J. Webb, *Nat. Geosci.*, 2015, **8**, 261–268.
3 J. H. Seinfeld, C. Bretherton, K. S. Carslaw, H. Coe, P. J. DeMott, E. J. Dunlea, G. Feingold, S. Ghan, A. B. Guenther, R. Kahn, I. Kraucunas, S. M. Kreidenweis, M. J. Molina, A. Nenes, J. E. Penner, K. A. Prather, V. Ramanathan, V. Ramaswamy, P. J. Rasch, A. R. Ravishankara, D. Rosenfeld, G. Stephens and R. Wood, *Proc. Natl. Acad. Sci.*, 2016, **113**, 5781–5790.
4 R. A. LaCour, J. P. Heindel, R. Zhao and T. Head-Gordon, *J. Am. Chem. Soc.*, 2025, **147**, 6299–6317.
5 Z. Wei, Y. Li, R. G. Cooks and X. Yan, *Annu. Rev. Phys. Chem.*, 2020, **71**, 31–51.
6 D. T. Holden, B. A. Shira, M. Q. Edwards, N. M. Morato and R. G. Cooks, *Chem. Sci.*, 2025, **16**, 17020–17033.
7 K. J. Vannoy, M. Q. Edwards, C. Renault and J. E. Dick, *Annu. Rev. Anal. Chem.*, 2024, **17**, 149–171.
8 B. Stevens and S. Bony, *Phys. Today*, 2013, **66**, 29–34.
9 J. K. Lee, K. L. Walker, H. S. Han, J. Kang, F. B. Prinz, R. M. Waymouth, H. G. Nam and R. N. Zare, *Proc. Natl. Acad. Sci.*, 2019, **116**, 19294–19298.
10 X. Li, X. Nong, C. Zhu, X. Gao, H. Chen, X. Yuan, D. Xing, L. Liu, C. Liang, D. Zang and X. Zhang, *J. Am. Chem. Soc.*, 2024, **146**, 29267–29271.

11 X. Chen, Y. Xia, Y. Yang, Y. Xu, X. Jia, R. N. Zare and F. Wang, *J. Am. Chem. Soc.*, 2024, **146**, 29742–29750.
12 C. Zhu, L. N. Pham, X. Yuan, H. Ouyang, M. L. Coote and X. Zhang, *J. Am. Chem. Soc.*, 2023, **145**, 21207–21212.
13 H. Kim and H.-C. Lim, *J. Phys. Chem. B*, 2015, **119**, 6740–6746.
14 H. Xiong, J. K. Lee, R. N. Zare and W. Min, *J. Phys. Chem. Lett.*, 2020, **11**, 7423–7428.
15 P. Prabhakaran, A. S. M. Shawon, G. Kinney, S. Thomas, W. Cantrell and R. A. Shaw, *Proc. Natl. Acad. Sci.*, 2020, **117**, 16831–16838.
16 M. Kaponig, A. Mölleken, H. Nienhaus and R. Möller, *Sci. Adv.*, 2021, **7**, eabg7595.
17 J. Li, Y. Xia, X. Song, B. Chen and R. N. Zare, *Proc. Natl. Acad. Sci.*, 2024, **121**, e2318408121.
18 Y. Xia, J. Li, Y. Zhang, Y. Yin, B. Chen, Y. Liang, G. Jiang and R. N. Zare, *Proc. Natl. Acad. Sci.*, 2023, **120**, e2302014120.
19 B. Chen, Y. Xia, R. He, H. Sang, W. Zhang, J. Li, L. Chen, P. Wang, S. Guo, Y. Yin, L. Hu, M. Song, Y. Liang, Y. Wang, G. Jiang and R. N. Zare, *Proc. Natl. Acad. Sci.*, 2022, **119**, e2209056119.
20 L. Qiu, X. Li, D. T. Holden and R. G. Cooks, *Chem. Sci.*, 2024, **15**, 12277–12283.
21 K. Lee, M. A. Mehrgardi and R. N. Zare, *J. Am. Chem. Soc.*, 2025, **147**, 33240–33247.
22 F. Wang, P. Yang, X. Tao, Y. Shi, S. Li, Z. Liu, X. Chen and Z. L. Wang, *ACS Nano*, 2021, **15**, 18206–18213.
23 J. P. Heindel, H. Hao, R. A. LaCour and T. Head-Gordon, *J. Phys. Chem. Lett.*, 2022, **13**, 10035–10041.
24 V. Towne, M. Will, B. Oswald and Q. Zhao, *Anal. Biochem.*, 2004, **334**, 290–296.
25 R. M. Sellers, *Analyst*, 1980, **105**, 950–954.
26 J. P. Heindel, R. A. LaCour and T. Head-Gordon, *Nat. Commun.*, 2024, **15**, 3670.
27 G. R. Eaton, S. S. Eaton, D. P. Barr and R. T. Weber, *Quantitative Epr*, Springer Science & Business Media, 2010.